photonics

MDPI

Article

Propagation Dynamics of Partially Coherent Perfect Vortex Beams in Biological Tissue Turbulence

Zhengguo Deng [1], Xiaohan Xie [2], Qian Pei [1], Jiale Yang [1], Zhimin Zhuo [1], Yufeng Shao [1], Jingping Xu [2] and Shuailing Wang [1,2,*]

[1] College of Information Science and Engineering, Jiaxing University, Jiaxing 314001, China; 00210750@stu.zjxu.edu.cn (Z.D.); 18833532880@163.com (Q.P.); 00206856@stu.zjxu.edu.cn (J.Y.); 19857333863@163.com (Z.Z.); syufeng@163.com (Y.S.)

[2] School of Physics Science and Engineering, Tongji University, Shanghai 200092, China; 2230980@tongji.edu.cn (X.X.); xx_jj_pp@tongji.edu.cn (J.X.)

* Correspondence: slwang@zjxu.edu.cn

Abstract

Based on the correlation function of partially coherent perfect vortex beams (PCPVBs) in biological tissue turbulence, a transmission model was established to systematically study how biological tissue and source parameters affect the received probability. Results indicate that the self-focusing property improves the received probability of PCPVBs during propagation, yielding a performance superior to that at the initial state. However, this enhancement effect gradually diminishes with decreasing turbulence strength. Owing to the perfect property, a similar received probability can be maintained at low-order orbital angular momentum (OAM), yet an inevitable degradation occurs as the OAM order further increases. The analysis also demonstrates that a beam configuration with a longer wavelength and a smaller ring radius can achieve superior transmission performance in biological tissue turbulence characterized by a shorter cut-off correlation length, smaller outer scale, and smaller fractal dimension. Furthermore, enlarging the receiving aperture reduces received probability; however, the declining trend levels off when the aperture is sufficiently large to collect the entire intensity information. This study unveils the propagation dynamics of PCPVBs in complex biological media, providing a crucial theoretical foundation and guidance for their applications in biological tissue optical communication, optical detection, and optical imaging.

Keywords: partially coherent perfect vortex beams; biological tissue turbulence; perfect property; self-focusing property; orbital angular momentum

Check for updates

Received: 1 September 2026
Revised: 20 September 2026
Accepted: 24 September 2026
Published: 29 September 2026

Copyright: © 2026 by the authors. Licensee MDPI, Basel, Switzerland. This article is an open access article distributed under the terms and conditions of the Creative Commons Attribution (CC BY) license.

1. Introduction

Laser technology, by virtue of its high brightness, monochromaticity, and directionality, has played an irreplaceable role in medical imaging, physiological parameter detection, and high-precision surgery, significantly enhancing the sensitivity of disease diagnosis and the minimally invasive nature of therapeutic procedures [1,2]. Consequently, the interaction between lasers and biological tissues has consistently remained a pivotal research frontier in the field of biophotonics [3–5]. However, as biomedical research progressively advances toward the cellular and even molecular scales, conventional Gaussian lasers have gradually revealed inherent limitations when addressing the demands of deep-tissue imaging, weak signal detection, and subcellular precision manipulation in complex biological environments. These limitations primarily stem from their restricted anti-scattering

capabilities, the diffraction-limited constraint on focal spot sizes, and the lack of tunable optomechanical degrees of freedom. Against this backdrop, vortex beams carrying orbital angular momentum (OAM) offer an entirely new physical dimension for overcoming the aforementioned limitations [6–9].

Vortex beams, benefiting from their unique self-focusing [10,11] and self-healing properties [12,13], exhibit a strong resistance to perturbations when propagating through turbulent media such as biological tissues, which is of considerable significance for improving the signal-to-noise ratio in deep-tissue bioimaging [14–16]. Meanwhile, the distinctive helical phase structure of their wavefronts imparts tunable OAM. This not only enables the rotation and trapping of microparticles [17], but also provides a novel encoding degree of freedom for biomedical optical communication [18–20]. Consequently, the introduction of vortex beams offers a highly promising and transformative technological pathway for biophotonics research. In recent years, perfect vortex beam (PVB), as a novel class of vortex optical fields, have attracted extensive attention owing to their unique perfect property that the beam size remains virtually invariant with respect to the OAM [21–23]. This distinctive property significantly improves transmission performance in applications such as optical communication [24–26], optical imaging [27,28], and optical detection [29]. Furthermore, recent studies have revealed that PVB also possess self-focusing and self-healing properties [30], which are expected to mitigate the perturbations induced by turbulent environments on their transmission quality, thereby enabling superior transmission performance.

Currently, most studies on PVB have theoretically modeled them as fully coherent optical fields [31,32]. However, constrained by practical optical components and energy limitations, the beams actually generated in experimental and engineering applications generally manifest as partially coherent perfect vortex beams (PCPVBs). Therefore, systematically investigating the propagation characteristics of PCPVBs in complex media holds substantial theoretical significance and practical value. This is particularly critical in biophotonics applications, where PCPVBs inevitably traverse biological tissue turbulence. This type of turbulence is composed of a vast number of interconnected microstructures with diverse morphologies [33,34]. Its inhomogeneous tissue architecture gives rise to a complex and irregular spatial distribution of the refractive index, thereby forming a chaotic system that is challenging to characterize precisely. When a PCPVB propagates through such a medium, the perturbations induced by biological tissue turbulence can significantly affect its transmission performance. Nevertheless, research on the propagation characteristics of PCPVBs in biological tissue turbulence remains largely unexplored, presenting a critical gap in the current literature.

In this article, we systematically investigate the evolution of the received probability for a PCPVB propagating through biological tissue turbulence. First, based on the field distribution of the PCPVB and the power spectrum of biological tissue turbulence, a correlation function is constructed to describe its transmission in turbulent media. This correlation function is then incorporated into the received probability analysis framework to establish a theoretical model for the transmission of a PCPVB in biological tissue turbulence. Finally, the evolutionary dynamics of the propagation behavior of PCPVBs in biological tissue turbulence are systematically analyzed through numerical simulations.

2. Transmission Model of a PCPVB in Biological Tissue Turbulence

The perfect vortex beam (PVB) possesses the remarkable property that its ring radius is almost independent of the topological charge m_0, and its complex amplitude at the source plane can be expressed as follows [35]:

$$E_P(\rho,\theta) = A_0 \exp\left(-\frac{\rho^2}{w_p^2}\right) I_{m_0}\left(\frac{2\rho r_0}{w_p^2}\right) \exp(im_0\theta), \quad (1)$$

where (ρ, θ) denotes the two-dimensional position vector; w_p is the Gaussian beam waist at the focus; I_{m_0} is the modified Bessel function of the first kind; and r_0 is defined as the ring radius of the PVB.

By invoking the extended Huygens–Fresnel principle, the complex amplitude of the PVB at the receiver plane located at distance z from the source plane in free space takes the following form:

$$E_P(r,\varphi,z) = -\frac{ik}{2\pi z}\exp(ikz)\int_0^{\infty}\int_0^{2\pi} E_P(\rho,\theta)\exp\left\{\frac{ik}{2z}\left[r^2+\rho^2-2r\rho\cos(\varphi-\theta)\right]\right\}\rho d\rho d\theta, \tag{2}$$

where $J_{m_0}(\cdot)$ represents the wave number, and λ is the wavelength of vortex beam.

Furthermore, with the assistance of the following mathematical integral expression,

$$\int_0^{2\pi}\exp\left[iv\widetilde{\theta}+ix\cos\left(\widetilde{\theta}-\theta\right)\right]d\widetilde{\theta} = i^v 2\pi\exp(iv\theta)J_v(x), \tag{3}$$

$$\int_0^{\infty}\exp\left(-nx^2\right)I_v(\alpha x)J_v(\beta x)xdx = \frac{1}{2n}\exp\left(\frac{\alpha^2-\beta^2}{4n}\right)J_v\left(\frac{\alpha\beta}{2n}\right), \tag{4}$$

$$\int_0^{\infty}\exp\left(-nx^2\right)J_v(\alpha x)J_v(\beta x)xdx = \frac{1}{2n}\exp\left(-\frac{\alpha^2+\beta^2}{4n}\right)I_v\left(\frac{\alpha\beta}{2n}\right), \tag{5}$$

the complex amplitude of the PVB upon propagation to a distance z in free space can be derived as follows:

$$E_P(r,\varphi,z) = -\frac{i^{m_0+1}kA_0}{2n_p z}\exp\left[i\left(kz+m_0\varphi+\frac{kr^2}{2z}\right)+\frac{\alpha_p^2-\beta_p^2}{4n_p}\right]J_{m_0}\left(\frac{\alpha_p\beta_p}{2n_p}\right), \tag{6}$$

with

$$n_p = \frac{1}{w_p^2}-\frac{ik}{2z},\ \alpha_p = \frac{2r_0}{w_p^2},\ \beta_p = -\frac{kr}{z},\ n_b = \frac{1}{w_b^2}-\frac{ik}{2z},\ \alpha_b = \frac{\eta}{w_b},\ \beta_b = -\frac{kr}{z}. \tag{7}$$

When optical signals propagate through biological tissue to communicate with an extracorporeal receiver, the highly inhomogeneous refractive index distribution of the tissue gives rise to severe turbulence-induced perturbations. The modified Rytov approximation is commonly employed to characterize such channels affected by turbulent fluctuations [18,36]. Within this framework, the cross-spectral density of a partially coherent perfect vortex beam (PCPVB) in biological tissue turbulence can be expressed via ensemble averaging as follows [37–39]:

$$\begin{aligned} W(r,r',\varphi,\varphi',z) &= u(r,\varphi,z)u^*(r',\varphi',z)_{pc,bio} \\ &= E_P(r,\varphi,z)E_p^*(r',\varphi',z) \\ &\times\langle\exp[i\psi(r,\varphi,z)-i\psi^*(r,\varphi',z)]\rangle_{pc} \\ &\times\langle\exp[\psi(r,\varphi,z)-\psi^*(r,\varphi',z)]\rangle_{bio}, \end{aligned} \tag{8}$$

where $\langle\cdot\rangle_{pc}$ is attributed to the inherent partial coherence of the source, and the coherence function $\langle\cdot\rangle_{bio}$ in the latter term arises from phase fluctuations in biological tissue turbulence, which can be respectively expressed as [37,40]:

$$\left\langle\exp\left[i\psi(r,\varphi,z)-i\psi^*(r,\varphi',z)\right]\right\rangle_{pc} = \exp\left\{-\frac{1}{\rho_{pc}^2}\left[r^2+r'^2-2rr'\cos(\varphi-\varphi')\right]\right\}, \tag{9}$$

$$\left\langle\exp\left[\psi(r,\varphi,z)-\psi^*(r,\varphi',z)\right]\right\rangle_{bio} = \exp\left\{-\frac{1}{\rho_{bio}^2}\left[r^2+r'^2-2rr'\cos(\varphi-\varphi')\right]\right\}, \tag{10}$$

where ρ_{pc} represents the coherence length of the partially coherent source, and for the case of $\rho_{pc} \to \infty$, the partially coherent vortex beam degenerates into a complete coherent vortex beam. ρ_{bio} denotes the spatial coherence radius of a spherical wave propagating through biological tissue turbulence, expressed as follows:

$$\rho_{bio} = \left[\frac{\pi^2 k^2 z}{3} \int_0^{1/l_{\max}} \kappa^3 \Phi_{bio}(\kappa) d\kappa \right]^{-1/2}. \tag{11}$$

Here, $\Phi_{bio}(\kappa)$ represents the spatial power spectrum of refractive index fluctuations for biological tissue turbulence, given by the following [41]:

$$\Phi_{bio}(\kappa) = \frac{\varepsilon^2 \eta_0 l_{\max}^{7-D_f}}{\pi^2 \left(7 - D_f\right)} \left(\frac{2}{L_0} \right)^{n-3/2} \frac{\Gamma(n)}{\Gamma(n - 3/2)\left(1 + \kappa^2 L_0^2\right)^n}, \tag{12}$$

where $\varepsilon^2 \eta_0 = 4n_0^4 (n_r - 1)^2 \eta_0$ represents the overall density of scattering centers, which is directly proportional to the radiographic density of the tissue, n_0 denotes the average refractive index of the biological tissue, n_r is the relative refractive index, $l_{\max}$ is defined as the cut-off correlation length, and D_f is related to the fractal dimension, and is $2n = 7 - D_f$ when $3 < D_f < 7$. L_0 represents the outer scale of the refractive index fluctuation structure, κ is the spatial wavenumber, and $\Gamma(\cdot)$ denotes the Gamma function.

By using the integral relation [18]

$$f_0^{\zeta} \frac{x^3}{(1 + \beta^2 x^2)^{\alpha}} dx = \frac{1 - \left(1 + \beta^2 \zeta^2\right)^{1-\alpha} \left[1 + \beta^2 \zeta^2 (\alpha - 1)\right]}{2\beta^4 (\alpha^2 - 3\alpha + 2)}, \tag{13}$$

we have

$$\rho_{bio} = \left\{ \frac{\pi^2 k^2 \left(\frac{2}{L_0}\right)^{n-3/2} \Gamma(n) z C_\varepsilon^2 \left\{ 1 - \left(1 + \frac{L_0^2}{l_{\max}^2}\right)^{1-n} \left[1 + (n-1)\frac{L_0^2}{l_{\max}^2}\right] \right\}}{6 L_0^4 (n^2 - 3n + 2) \Gamma\left(n - \frac{3}{2}\right)} \right\}^{-1/2}. \tag{14}$$

and here $C_\varepsilon^2 = \frac{\varepsilon^2 \eta_0 l_{\max}^{7-D_f}}{\pi^2 \left(7 - D_f\right)}$.

Given that an arbitrary vortex beam can be synthesized as a superposition of helical harmonics $\exp(i m_0 \varphi)$ in cylindrical coordinates, the probability density of the signal OAM mode, which characterizes the OAM content of a vortex beam upon propagation through biological tissue turbulence, can be written as follows [42]:

$$\left\langle \left| a_{p,m}(r,z) \right|^2 \right\rangle = \frac{1}{2\pi} \int_0^{2\pi} \int_0^{2\pi} R(r, r', \varphi, \varphi', z) \exp\left[-im(\varphi - \varphi') \right] d\varphi d\varphi'. \tag{15}$$

By substituting Equations (8), (11) and (12) into Equation (13), the probability density distribution of a PCPVB propagating through biological tissue turbulence can be obtained as follows:

$$\begin{aligned} \left\langle \left| a_{p,m}(r,z) \right|^2 \right\rangle = {} & \frac{1}{2\pi} \int_0^{2\pi} \int_0^{2\pi} \frac{k^2 A_0^2}{4 n_p n_p^* z^2} \exp[i(m_0 - m)(\varphi - \varphi')] J_{m_0}\left(\frac{\alpha_p \beta_p}{2 n_p} \right) J_{m_0}\left(\frac{\alpha_p \beta_p}{2 n_p^*} \right) \\ & \exp\left(\frac{\alpha_p^2 - \beta_p^2}{4 n_p} + \frac{\alpha_p^2 - \beta_p^2}{4 n_p^*} \right) \exp\left[-\frac{2r^2 - 2r^2 \cos(\varphi - \varphi')}{\rho_{bio}^2} \right] \exp\left[-\frac{2r^2 - 2r^2 \cos(\varphi - \varphi')}{\rho_{pc}^2} \right] d\varphi d\varphi'. \end{aligned} \tag{16}$$

With the aid of the following integral formula,

$$\int_0^{2\pi} \exp\left[-iy\varphi + x\cos(\varphi - \varphi')\right] d\varphi = 2\pi \exp(-iy\varphi') I_y(x), \tag{17}$$

the integral expression for the probability density distribution can be converted into a more computationally accessible analytical expression:

$$\begin{aligned} \left\langle \left| a_{p,m}(r,z) \right|^2 \right\rangle = \frac{k^2 A_0^2}{4 n_p n_p^* z^2} \exp\left[\frac{\alpha_p^2 - \beta_p^2}{4 n_p} + \frac{\alpha_p^2 - \beta_p^2}{4 n_p^*} - 2r^2 \left(\frac{1}{\rho_{bio}^2} + \frac{1}{\rho_{pc}^2} \right) \right] \\ J_{m_0}\left(\frac{\alpha_p \beta_p}{2 n_p} \right) J_{m_0}\left(\frac{\alpha_p \beta_p}{2 n_p^*} \right) I_{m-m_0}\left[2r^2 \left(\frac{1}{\rho_{bio}^2} + \frac{1}{\rho_{pc}^2} \right) \right]. \end{aligned} \tag{18}$$

Integrating the probability density distribution over the full receiving aperture yields the conditional modal probability of the transmitted mode, given by the following:

$$P(m|m_0) = \frac{\int_0^{D/2} \left\langle \left| a_{p,m}(r,z) \right|^2 \right\rangle r dr}{\sum_{m=-\infty}^{\infty} \int_0^{D/2} \left\langle \left| a_{p,m}(r,z) \right|^2 \right\rangle r dr}, \tag{19}$$

where D is the receiving aperture; the diagonal term $P(m|m_0)$ corresponds to the received probability; and the off-diagonal terms $P(m|m_0)$ for $m_0 \neq m$ represent the crosstalk probability between OAM modes. Therefore, $P(m|m_0)$ can also be characterized as the detection probability of the beam.

3. Numerical Simulation

In this section, the propagation characteristics of PCPVBs in biological tissue turbulence are investigated through numerical simulations of the detection probability. Unless otherwise specified, the following parameters for the beam source and biological tissue turbulence are adopted [43–45]: $\lambda = 1550$ nm, $r_0 = 0.05$ mm, $z = 0.6$ mm, $m_0 = 1$, $m = 1$, $D_f = 10/3$, $n = 11/6$, $L_0 = 0.0026$ mm, $w_p = 0.005$ mm, $l_{\max} = 0.003$ mm, $\varepsilon^2 \eta_0 = 9.854 \times 10^{-4}$, $\rho_{pc} = 0.001$ m, $D_0 = 0.3$ mm.

The partial coherence properties of PCPVBs exert a profound influence on their propagation behavior through biological tissue turbulence. Figure 1 illustrates the evolution of the received probability as a function of the coherence length. As the coherence length increases, the received probability of the PCPVB improves continuously, indicating that a fully coherent beam outperforms a partially coherent beam in terms of communication performance over short-distance transmission. This is because the received probability reflects the receiver's capability to detect the purity of the OAM mode. Benefiting from its high initial mode purity, a fully coherent beam can maintain an elevated received probability during the early stages of propagation. In contrast, the limited initial coherence of a partially coherent beam results in a lower mode purity, causing a portion of its energy to be partially coupled into adjacent OAM modes already at the transmitter. Consequently, its received probability remains lower than that of fully coherent beams throughout subsequent propagation. Furthermore, it can also be observed from Figure 1, the inherent self-focusing property of PCPVBs facilitates a partial recovery of the received probability during propagation, enabling PCPVBs to even surpass their initial received probability. This is mainly attributed to the fact that the PCPVB inherits the unique self-focusing property of the PVB, which causes the beam to contract and the intensity to refocus during propagation. The refocused intensity leads to a certain recovery of the received probability of the PCPVB. This observation also indicates that, in practical applications of the PCPVB, the position of the receiving plane should be properly selected so that it is located at the secondary

maximum of the recovered received probability, thereby maximizing the recovery effect enabled by the self-focusing property of the PCPVB.

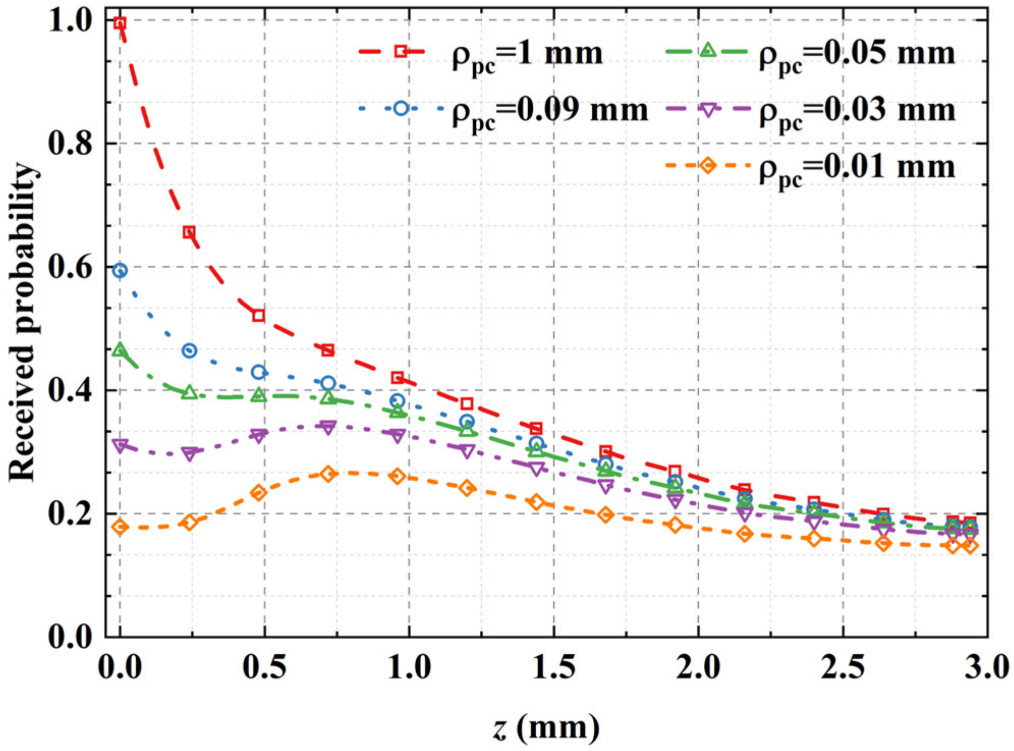


Figure 1. Evolution of the received probability of PCPVBs with propagation distance under different coherence lengths.

In optical communication and detection applications within biological tissue turbulence, the propagation performance of PCPVBs is highly contingent upon the optimal configuration of source beam parameters. In theoretical studies of biological tissue optics, the operating wavelength band is typically selected within the range of 850–1550 nm. Figure 2 illustrates the influence of the operating wavelength and the ring radius on the propagation performance of PCPVBs in biological tissue turbulence. The analysis results demonstrate that as the operating wavelength increases, the transmission performance of the PCPVB becomes increasingly superior. The underlying physical mechanism lies in the fact that longer wavelengths exhibit enhanced diffraction properties and penetration capabilities. This enables the beam to traverse biological tissue turbulence more effectively, thereby delivering the signal to the receiver with higher fidelity and intensity. It should be noted that our theoretical derivation framework does not consider the absorption effect of biological tissue turbulence. It can also be observed from Figure 2 that as the ring radius of the PCPVB increases, its received probability declines continuously, and the transmission performance degrades progressively. This is primarily attributable to the fact that the ring radius directly determines the transverse spatial scale of the beam. When a beam with a larger size traverses biological tissue turbulence characterized by random refractive index fluctuations, it becomes more susceptible to perturbations induced by turbulent eddy structures, resulting in aggravated wavefront distortion and intensified modal crosstalk, which in turn causes a deterioration in the signal quality at the receiver. Therefore, when applying PCPVBs to optical communication or detection systems operating in biological tissue turbulence, a parameter combination consisting of a longer operating wavelength and a smaller ring radius should be preferentially selected to minimize turbulence-induced effects to the greatest extent possible and to ensure efficient and stable signal transmission.

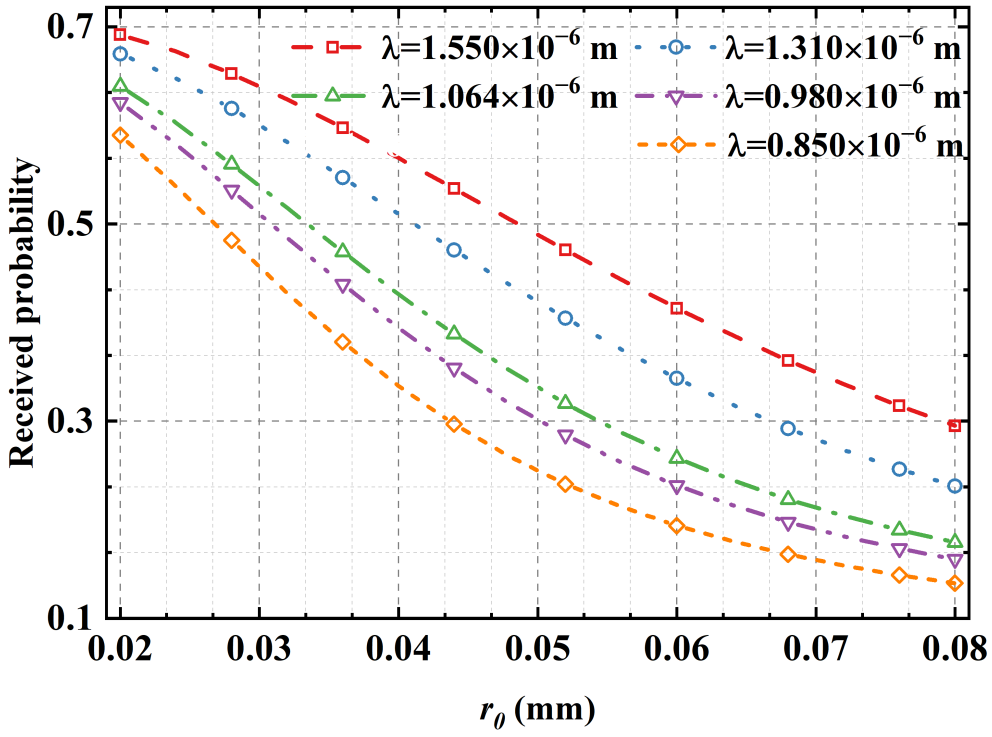


Figure 2. Variation in the received probability of PCPVBs with the ring radius under different wavelengths.

Biological tissue turbulence consists of interconnected irregular turbulent eddies whose length scales span multiple orders of magnitude. Consequently, it can be modeled as a continuous random medium characterized by a multi-scale fractal structure. Within this framework, the truncated correlation length and the outer scale of the fractal behavior serve as critical parameters for characterizing the structural properties of biological tissues. Figure 3 illustrates the influence of the cut-off correlation length and the outer scale on the propagation performance of a PCPVB. As shown in Figure 3, the received probability of the PCPVB increases as the cut-off correlation length decreases. This phenomenon is primarily attributable to the fact that the cut-off correlation length represents the largest structural correlation scale in the biological medium. A reduction in the cut-off correlation length implies that the permittivity fluctuations become correlated over shorter distances, thereby lowering the overall turbidity and facilitating the propagation of the PCPVB [46]. Figure 3 also demonstrates that an increase in the outer scale leads to a degradation of PCPVB transmission performance. This deterioration occurs because the outer scale characterizes the scale at which the correlation function transitions into a power-law decay regime. A larger outer scale extends the range over which the refractive index fluctuations remain correlated, giving rise to a more complex turbulent environment and consequently resulting in poorer propagation performance of the PCPVB [47].

The self-focusing property of perfect vortex beam has attracted considerable attention in recent years, owing to its ability to effectively enhance the beam's performance over long-distance propagation and to enable a certain degree of recovery in the received probability degraded by turbulence during propagation. Figure 4 investigates the self-focusing property of a PCPVB. The results demonstrate that the PCPVB inherits the self-focusing behavior of perfect vortex beam, enabling the recovery of the received probability in relatively strong turbulence environments. Moreover, Figure 4 further reveals that as the fractal dimension decreases, the self-focusing property of the PCPVB becomes progressively less pronounced. This phenomenon can be attributed to the fact that fractal dimension, as a non-integer

dimension describing the complexity and space-filling capacity of a geometric object, quantifies the structural self-similarity and irregularity. A decrease in fractal dimension signifies a reduction in the complexity and irregularity of the biological tissue structure, leading to a smoother turbulent environment. Under weak turbulence conditions, the PCPVB can maintain its profile relatively well, and the self-focusing phenomenon is comparatively gentle and difficult to observe distinctly. In contrast, under strong turbulence conditions, the severe beam spreading and distortion induced by turbulence cause the self-focusing property to be significantly triggered and highlighted as a compensatory mechanism.

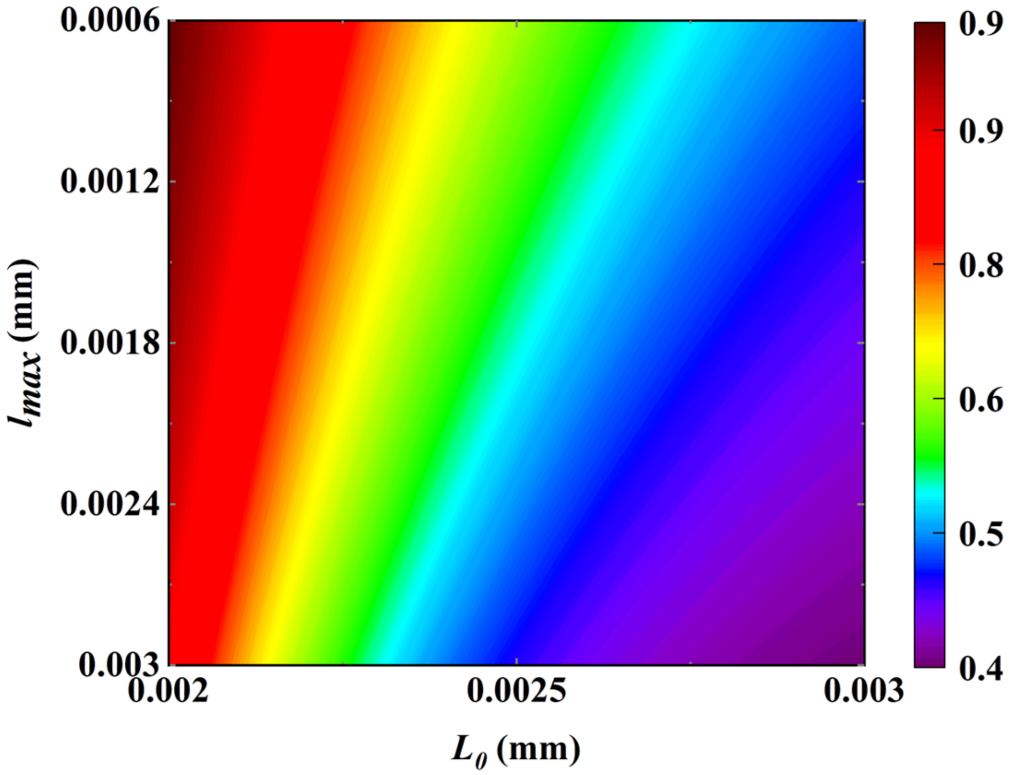


Figure 3. Trend of the variation in the received probability of PCPVBs under the influence of the cut-off correlation length and the outer scale of biological tissue turbulence. The color bar represents the received probability.

In practical applications such as optical detection, communication, and imaging, the optimization of the receiving aperture is critical to the transmission performance of PCPVB. Figure 5a investigates the influence of the receiving aperture and the OAM on the received probability of PCPVBs at $z = 0.3$ mm. To avoid infinite summation for the conditional modal probability of the PVB, we set the OAM order range from $m_0 - 10$ to $m_0 + 10$. As illustrated in Figure 5a, the received probability of PCPVBs progressively improves as the receiving aperture decreases. This phenomenon is primarily attributed to the unique ring-shaped intensity distribution of PCPVB. When the receiving aperture is reduced, the detector predominantly collects the highly localized intensity component at the center of the ring. This specific component exhibits relatively high stability against turbulence, thereby yielding a higher received probability. As the receiving aperture increases, the intensity components in the peripheral region, which are more susceptible to turbulence perturbations, are also included in the reception, resulting in a decline in the received probability. Notably, when the receiving aperture is further enlarged to the point where the entire beam intensity is captured, the degradation trend of the received probability gradually plateaus. Furthermore, Figure 5a reveals the dependence of the received probability on the OAM mode. Benefiting from the inherent perfect property of

PCPVB, the received probability remains virtually insensitive to variations in the OAM mode at low orders. However, as the OAM mode increases further, the received probability inevitably experiences a decline. Figure 5b shows the detection probability distribution of the PCPVB in biological tissue turbulence under different m_0 and m. It can be observed that, due to the temporal and spatial variations in the refractive index distribution in biological tissue turbulence, the signal OAM state leaks into adjacent OAM modes, resulting in significant crosstalk between different OAM channels. The maximum crosstalk probability can be observed in the channels with $m_0 - m = \pm 1$, because the large-scale energy induced by turbulence spills over into the adjacent OAM channels. However, owing to the perfect property of the PCPVB, the crosstalk probability of its adjacent OAM channels does not further increase with changes in the signal OAM state.

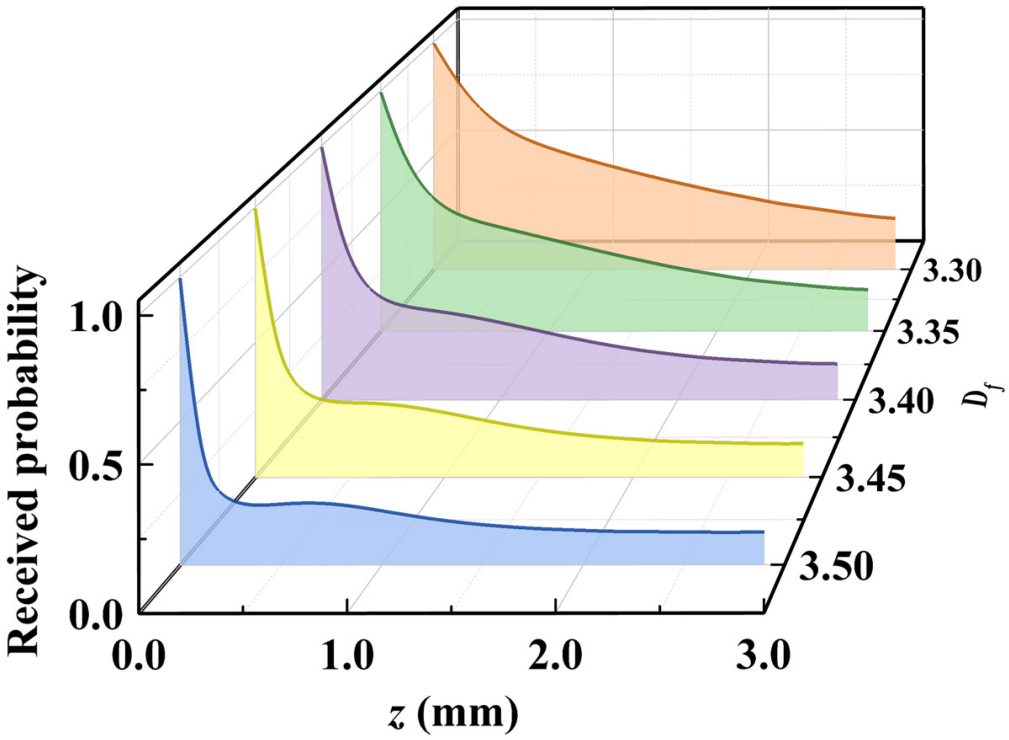


Figure 4. Influence of different fractal dimensions on the evolution trend of the received probability of PCPVB.

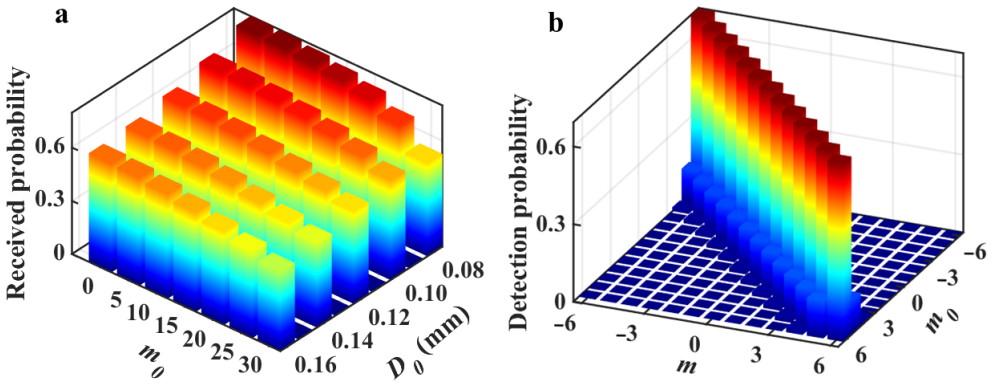


Figure 5. (**a**) Dependence of the received probability of PCPVBs on the OAM mode and receiving aperture. (**b**) The detection probability of PCPVBs varies with different values of m_0 and m.

4. Discussion

In recent years, numerous studies have been conducted on the propagation of fully coherent perfect vortex beams in free-space [48], atmospheric turbulence [49,50], and oceanic turbulence [51]. Nevertheless, restricted by practical constraints such as light-source energy and optical-component performance, the beams generated in real optical systems are usually PCPVB. Meanwhile, with the rapid development of biomedical photonics, it is urgent to understand the propagation evolution law of PCPVBs under biological tissue turbulence. Against this backdrop, this study carries out numerical simulations on the propagation of PCPVBs in biological tissue turbulence. The simulation results demonstrate that the self-focusing property of PCPVBs can compensate for turbulence-induced mode crosstalk, enabling a received probability higher than the initial value under strong biological tissue turbulence. Enlarging the receiving aperture leads to a reduction in received probability; however, this decreasing trend levels off once the aperture is large enough to capture the full annular intensity information. Corresponding experimental verification can be implemented based on the simulation results: a near-infrared laser illuminates a spatial light modulator (SLM), where a composite phase mask is loaded to generate PCPVB. The beam then passes through a second SLM loaded with phase screens for biological tissue turbulence, or real biological tissue slices are adopted to simulate turbulent disturbances. By adjusting the ring radius and ring thickness of PCPVB, a CCD detector can capture the complete output light-field. It should be noted that the detector aperture needs to match the ring-shaped beam spot broadened after turbulence interaction.

5. Conclusions

In summary, by establishing a propagation model for PCPVBs in biological tissue turbulence and conducting comprehensive numerical simulations, this study systematically investigates the impacts of biological tissue turbulence characteristics and source parameters on the received probability of the beams. The results demonstrate that, benefiting from the unique self-focusing property of the PCPVB, a received probability superior to that at the initial state can be attained during propagation through biological tissue turbulence. Under weak turbulence conditions, the self-focusing property is not easily discernible due to limited turbulence-induced perturbations; however, as the turbulence strength increases, the self-focusing property becomes progressively more prominent and constitutes a significant factor influencing the received probability. Furthermore, the inherent perfect property of PCPVBs renders their transmission performance virtually insensitive to variations in the OAM mode at low orders. Nevertheless, as the OAM mode increases further, the received probability inevitably exhibits a degradation trend. Investigation at the received end reveals that an enlarged aperture admits more peripheral intensity components susceptible to turbulence-induced phase perturbations into the detection range, leading to a reduction in the received probability. However, this degradation trend gradually plateaus once the aperture is sufficiently large to capture the entire beam intensity. It should be noted that the received probability here characterizes the conditional OAM-mode probability rather than the overall transmission efficiency of the beam. Therefore, the improvement in modal purity achieved by reducing the aperture comes at the cost of a decreased overall transmission efficiency. Further studies indicate that under the assumption of neglected absorption, PCPVBs configured with a longer wavelength and a smaller ring radius can achieve superior transmission performance in biological tissue turbulence characterized by a shorter cut-off correlation length, a smaller outer scale, and a smaller fractal dimension. This study deepens the understanding of the interaction mechanisms between PCPVBs and biological tissues within the field of biophotonics, and provides a crucial theoretical

foundation and guidance for technological applications such as optical communication, optical detection, and optical imaging in biomedicine.

Author Contributions: Conceptualization, S.W. and X.X.; methodology, S.W. and Q.P.; software, S.W.; formal analysis, Z.D. and J.Y.; writing—original draft preparation, S.W. and X.X.; writing—review and editing, S.W., Z.D. and Z.Z.; funding acquisition, S.W., J.X. and Y.S. All authors have read and agreed to the published version of the manuscript.

Funding: This research was funded by the National Natural Science Foundation of China (12174288, 12274326, 12174243, 61905186); National Key Research and Development Program of China (2021YFA1400602); Shanghai Aerospace Science and Technology Innovation Foundation (SAST-2022-069); and Fundamental Research Funds for the Central Universities (ZYTS23078).

Institutional Review Board Statement: Not applicable.

Informed Consent Statement: Not applicable.

Data Availability Statement: Data are available on request from the authors.

Conflicts of Interest: The authors declare no conflicts of interest.

References

1. Paterson, L.; MacDonald, M.P.; Arlt, J.; Sibbett, W.; Bryant, P.E.; Dholakia, K. Controlled rotation of optically trapped microscopic particles. *Science* **2001**, *292*, 912–914. [CrossRef] [PubMed]
2. Jia, S.; Vaughan, J.C.; Zhuang, X. Isotropic 3D Super-resolution Imaging with a Self-bending Point Spread Function. *Nat. Photonics* **2014**, *8*, 302–306. [CrossRef] [PubMed]
3. Wang, Z.; Zhu, L.; Zhang, H.; Li, G.; Yi, C.; Li, Y.; Yang, Y.; Ding, Y.; Zhen, M.; Gao, S.; et al. Real-time volumetric reconstruction of biological dynamics with light-field microscopy and deep learning. *Nat. Methods* **2021**, *18*, 551–556. [CrossRef] [PubMed]
4. Gao, L.; Shao, L.; Chen, B.C.; Betzig, E. 3D live fluorescence imaging of cellular dynamics using Bessel beam plane illumination microscopy. *Nat. Protoc.* **2014**, *9*, 1083–1101. [CrossRef] [PubMed]
5. Guo, X.; Zhao, F.; Zhu, J.; Zhu, D.; Zhao, Y.; Fei, P. Rapid 3D isotropic imaging of whole organ with double-ring light-sheet microscopy and self-learning side-lobe elimination. *BioMed Opt. Express* **2023**, *14*, 6206–6221. [CrossRef] [PubMed]
6. Shen, Y.; Wang, X.; Xie, Z.; Min, C.; Fu, X.; Liu, Q.; Gong, M.; Yuan, X. Optical vortices 30 years on: OAM manipulation from topological charge to multiple singularities. *Light Sci. Appl.* **2019**, *8*, 90. [CrossRef] [PubMed]
7. Yao, A.M.; Padgett, M.J. Orbital angular momentum: Origins, behavior and applications. *Adv. Opt. Photon.* **2011**, *3*, 161–204. [CrossRef]
8. Willner, A.E.; Huang, H.; Yan, Y.; Ren, Y.; Ahmed, N.; Xie, G.; Bao, C.; Li, L.; Cao, Y.; Zhao, Z.; et al. Optical communications using orbital angular momentum beams. *Adv. Opt. Photon.* **2015**, *7*, 66–106. [CrossRef]
9. Singh, S.K. Restoring modal orthogonality in asymmetric Tricomi beams for Conjugate-Keyed Mode Division Multiplexing. *Opt. Commun.* **2026**, *616*, 133345. [CrossRef]
10. Mei, Z.; Korotkova, O.; Zhao, D.; Mao, Y. Self-focusing vortex beams. *Opt. Lett.* **2021**, *46*, 2384–2387. [CrossRef] [PubMed]
11. Wang, L.; Ji, X.; Deng, Y.; Li, X.; Wang, T.; Fan, X.; Yu, H. Self-focusing effect on the characteristics of Airy beams. *Opt. Commun.* **2019**, *441*, 190–194. [CrossRef]
12. Wang, L.; Ji, X.; Li, X.; Wang, T.; Yu, H.; Li, Q. Focusing and self-healing characteristics of Airy array beams propagating in self-focusing media. *Appl. Phys. B* **2019**, *125*, 165. [CrossRef]
13. Garces-Chavez, V.; McGloin, D.; Melville, H.; Sibbett, W.; Dholakia, K. Simultaneous micromanipulation in multiple planes using a self-reconstructing light beam. *Nature* **2002**, *419*, 145–147. [CrossRef] [PubMed]
14. Shen, Y.; Pidishety, S.; Nape, I.; Dudley, A. Self-healing of structured light: A review. *J. Opt.* **2022**, *24*, 103001. [CrossRef]
15. Rubinsztein-Dunlop, H.; Forbes, A.; Berry, M.V.; Dennis, M.R.; Andrews, D.L.; Mansuripur, M.; Denz, C.; Alpmann, C.; Banzer, P.; Bauer, T.; et al. Roadmap on structured light. *J. Opt.* **2017**, *19*, 6. [CrossRef]
16. Chen, J.; Sasaki, H.; Lai, H.; Su, Y.; Liu, J.; Wu, Y.; Zhovmer, A.; Combs, C.A.; Rey-Suarez, I.; Chang, H.Y.; et al. Three-dimensional residual channel attention networks denoise and sharpen fluorescence microscopy image volumes. *Nat. Methods* **2021**, *18*, 678–687. [CrossRef] [PubMed]
17. Zhang, P.; Prakash, J.; Zhang, Z.; Mills, M.S.; Efremidis, N.K.; Christodoulides, D.N.; Chen, Z. Trapping and guiding microparticles with morphing autofocusing Airy beams. *Opt. Lett.* **2011**, *36*, 2883–2885. [CrossRef] [PubMed]
18. Chen, M.; Yu, L.; Zhang, Y. Signal/noise ratio of orbital angular momentum modes for a partially coherent modified Bessel-correlated beam in a biological tissue. *J. Opt. Soc. Am. A Opt. Image. Sci. Vis.* **2017**, *34*, 2046–2051. [CrossRef] [PubMed]

19. Li, Y.; Zhang, Y.; Zhu, Y.; Yu, L. Modified biological spectrum and SNR of Laguerre-Gaussian pulsed beams with orbital angular momentum in turbulent tissue. *Opt. Express* **2019**, *27*, 9749–9762. [CrossRef] [PubMed]
20. Meyer, J.; Reches, Y.; Gary Rozenman, G.; Oz, Y.; Suchowski, H.; Arie, A. Analogy of free-space quantum key distribution using spatial modes of light: Scaling up the distance and the dimensionality. *Opt. Lett.* **2025**, *50*, 3297–3300. [CrossRef]
21. Ostrovsky, A.S.; Rickenstorff-Parrao, C.; Arrizon, V. Generation of the "perfect" optical vortex using a liquid-crystal spatial light modulator. *Opt. Lett.* **2013**, *38*, 534–536. [CrossRef] [PubMed]
22. Vaity, P.; Rusch, L. Perfect vortex beam: Fourier transformation of a Bessel beam. *Opt. Lett.* **2015**, *40*, 597–600. [CrossRef] [PubMed]
23. Zhu, F.; Huang, S.; Shao, W.; Zhang, J.; Chen, M.; Zhang, W.; Zeng, J. Free-space optical communication link using perfect vortex beams carrying orbital angular momentum (OAM). *Opt. Commun.* **2017**, *396*, 50–57. [CrossRef]
24. Yang, C.; Lan, Y.; Jiang, X.; Long, H.; Hou, J.; Chen, S. Beam-holding property analysis of the perfect optical vortex beam transmitting in atmospheric turbulence. *Opt. Commun.* **2020**, *472*, 125879. [CrossRef]
25. Wang, S.; Wang, J.; Yang, Y.; Xu, J.; Wang, L.-G. Robust Visible Light Communication via Perfect Vortex Beams. *J. Light. Technol.* **2025**, *43*, 7572–7579. [CrossRef]
26. Xu, X.; Luo, C.; Qian, X.; Zhu, W. Investigation of the Propagation Characteristics of Double-Ring Perfect Vortex Beams in Atmospheric Turbulence. *Photonics* **2024**, *11*, 768. [CrossRef]
27. Zhang, C.; Min, C.; Du, L.; Yuan, X.C. Perfect optical vortex enhanced surface plasmon excitation for plasmonic structured illumination microscopy imaging. *Appl. Phys. Lett.* **2016**, *108*, 201601. [CrossRef]
28. Chen, Y.; Fang, Z.X.; Ren, Y.X.; Gong, L.; Lu, R.D. Generation and characterization of a perfect vortex beam with a large topological charge through a digital micromirror device. *Appl. Opt.* **2015**, *54*, 8030–8035. [CrossRef] [PubMed]
29. Chen, M.; Mazilu, M.; Arita, Y.; Wright, E.M.; Dholakia, K. Dynamics of microparticles trapped in a perfect vortex beam. *Opt. Lett.* **2013**, *38*, 4919–4922. [CrossRef] [PubMed]
30. Wang, S.; Wang, J.; Cheng, M.; Zhang, J.; Yang, X.; Xu, J.; Wang, L.-G. Three transmission properties of the perfect vortex beam. *Opt. Express* **2024**, *32*, 34141–34152. [CrossRef] [PubMed]
31. Kumar Das, B.; Granados, C.; Ciappina, M.F. Generation of elliptical perfect optical vortex beams and their propagation in free-space. *Appl. Opt.* **2024**, *63*, 2737–2745. [CrossRef] [PubMed]
32. Abd El-Mottaleb, S.A.; Bencheikh, A. Perfect vortex Laguerre-Gauss beams as a carrier in the MMF/FSO communication system. *Appl. Opt.* **2024**, *63*, 5931–5938. [CrossRef]
33. Zhang, H.; Cui, Z.; Han, Y.; Guo, J.; Chang, C. Average Intensity and Beam Quality of Hermite-Gaussian Correlated Schell-Model Beams Propagating in Turbulent Biological Tissue. *Front. Phys.* **2021**, *9*, 650537. [CrossRef]
34. Power, R.M.; Huisken, J. A guide to light-sheet fluorescence microscopy for multiscale imaging. *Nat. Methods* **2017**, *14*, 360–373. [CrossRef] [PubMed]
35. Wang, S.; Cheng, M.; Yang, X.; Xu, J.; Yang, Y. Self-focusing effect analysis of a perfect optical vortex beam in atmospheric turbulence. *Opt. Express* **2023**, *31*, 20861–20871. [CrossRef] [PubMed]
36. Baykal, Y. Field correlations of a partially coherent optical Gaussian wave in tissue turbulence. *J. Opt. Soc. Am. A Opt. Image. Sci. Vis.* **2022**, *39*, C6–C11. [CrossRef] [PubMed]
37. Ou, J.; Yin, Z.; Chi, H.; Li, Q.; Yang, B.; Yang, S.; Zhai, Y. Partially coherent anomalous vortex beam in anisotropic turbulence. *Opt. Commun.* **2023**, *537*, 129411. [CrossRef]
38. Cheng, M.; Zhang, Y.; Zhu, Y.; Gao, J.; Dan, W.; Hu, Z.; Zhao, F. Effects of non-Kolmogorov turbulence on the orbital angular momentum of Hankel–Bessel–Schell beams. *Opt. Laser Technol.* **2015**, *67*, 20–24. [CrossRef]
39. Yun Zhu, Y.Z.; Licheng Zhang, L.Z.; Zhang, Y. Spiral spectrum of Airy–Schell beams through non-Kolmogorov turbulence. *Chin. Opt. Lett.* **2016**, *14*, 042101–042105. [CrossRef]
40. Li, Y.; Han, Y.; Cui, Z.; Hui, Y. Performance analysis of the OAM based optical wireless communication systems with partially coherent elegant Laguerre–Gaussian beams in oceanic turbulence. *J. Opt.* **2019**, *21*, 035702. [CrossRef]
41. Wu, Y.; Zhang, Y.; Wang, Q.; Hu, Z. Average intensity and spreading of partially coherent model beams propagating in a turbulent biological tissue. *J. Quant. Spectrosc. Radiat. Transf.* **2016**, *184*, 308–315. [CrossRef]
42. Yang, H.; Yan, Q.; Zhang, Y.; Hu, L. Received probability of perfect optical vortex in absorbent and weak turbulent seawater links. *Appl. Opt.* **2021**, *60*, 10772–10779. [CrossRef] [PubMed]
43. Paterson, C. Atmospheric turbulence and orbital angular momentum of single photons for optical communication. *Phys. Rev. Lett.* **2005**, *94*, 153901. [CrossRef] [PubMed]
44. Chen, C.Y.; Yang, H.M.; Tong, S.F.; Ren, B.; Li, Y.F. Characterization of temporal pulse broadening for horizontal propagation in strong anisotropic atmospheric turbulence. *Opt. Express* **2015**, *23*, 4814–4828. [CrossRef] [PubMed]
45. Korotkova, O.; Wolf, E. Beam criterion for atmospheric propagation. *Opt. Lett.* **2007**, *32*, 2137–2139. [CrossRef] [PubMed]
46. Xu, M.; Alfano, R.R. Fractal mechanisms of light scattering in biological tissue and cells. *Opt. Lett.* **2005**, *30*, 3051–3053. [CrossRef] [PubMed]
47. Sheppard, C.J. Fractal model of light scattering in biological tissue and cells. *Opt. Lett.* **2007**, *32*, 142–144. [CrossRef] [PubMed]

48. Sivarajan, A.K.; Vardhan, H.; Choudhary, S.; Reddy, S.G.; Kumar, R. Free space evolution of perfect optical vortices through interferometric analysis. *Opt. Lasers Eng.* **2025**, *194*, 109178. [CrossRef]
49. Reis, G.B.; Gesualdi, M.R.R. Characterization of turbulence effects in perfect optical vortex via holographic techniques. *Appl. Opt.* **2025**, *64*, 3833–3841. [CrossRef] [PubMed]
50. Qin, Y. Efficient and low-crosstalk propagation of perfect vortex beams in free space and atmospheric turbulence. *Opt. Express* **2025**, *33*, 45602–45614. [CrossRef] [PubMed]
51. Hu, Z.; Liu, H.; Xia, J.; He, A.; Li, H.; Du, Z.; Chen, T.; Li, Z.; Lu, Y. Propagation characteristics of the perfect vortex beam in anisotropic oceanic turbulence. *Appl. Opt.* **2020**, *59*, 9956–9962. [CrossRef] [PubMed]

Disclaimer/Publisher's Note: The statements, opinions and data contained in all publications are solely those of the individual author(s) and contributor(s) and not of MDPI and/or the editor(s). MDPI and/or the editor(s) disclaim responsibility for any injury to people or property resulting from any ideas, methods, instructions or products referred to in the content.